1-1-2011

Reactions of simple and peptidic alpha-carboxylate radical anions with dioxygen in the gas phase

Tony Ly
University of Wollongong, tly@uow.edu.au

Benjamin B. Kirk
University of Wollongong, bkirk@uow.edu.au

Pramesh I. Hettiarachchi
University of Wollongong

Berwyck L. Poad
Ucsd (University California, Sand Diego), bpoad@uow.edu.au

Adam J. Trevitt
University of Wollongong, adamt@uow.edu.au

See next page for additional authors

Reactions of simple and peptidic alpha-carboxylate radical anions with dioxygen in the gas phase

Abstract

α-Carboxylate radical anions are potential reactive intermediates in the free radical oxidation of biological molecules (e.g., fatty acids, peptides and proteins). We have synthesised well-defined α-carboxylate radical anions in the gas phase by UV laser photolysis of halogenated precursors in an ion-trap mass spectrometer. Reactions of isolated acetate (CH2CO 2-) and 1-carboxylatobutyl (CH3CH 2CH2CHCO2-) radical anions with dioxygen yield carbonate (CO3-) radical anions and this chemistry is shown to be a hallmark of oxidation in simple and alkyl-substituted cross-conjugated species. Previous solution phase studies have shown that Cα-radicals in peptides, formed from free radical damage, combine with dioxygen to form peroxyl radicals that subsequently decompose into imine and keto acid products. Here, we demonstrate that a novel alternative pathway exists for two α-carboxylate Cα-radical anions: the acetylglycinate radical anion (CH3C(O)NHCHCO2-) and the model peptide radical anion, YGGFG-. Reaction of these radical anions with dioxygen results in concerted loss of carbon dioxide and hydroxyl radical. The reaction of the acetylglycinate radical anion with dioxygen reveals a two-stage process involving a slow, followed by a fast kinetic regime. Computational modelling suggests the reversible formation of the Cα peroxyl radical facilitates proton transfer from the amide to the carboxylate group, a process reminiscent of, but distinctive from, classical proton-transfer catalysis. Interestingly, inclusion of this isomerization step in the RRKM/ME modelling of a G3SX level potential energy surface enables recapitulation of the experimentally observed two-stage kinetics. © 2011 the Owner Societies

Keywords

reactions, simple, peptidic, phase, alpha, gas, carboxylate, radical, anions, dioxygen, GeoQUEST

Disciplines

Life Sciences | Physical Sciences and Mathematics | Social and Behavioral Sciences

Publication Details

Ly, T., Kirk, B. B., Hettiarachchi, P. I., Poad, B. L., Trevitt, A. J., da Silva, G. & Blanksby, S. J. (2011). Reactions of simple and peptidic alpha-carboxylate radical anions with dioxygen in the gas phase. Physical Chemistry Chemical Physics, 13 (36), 16314-16323.

Authors

Tony Ly, Benjamin B. Kirk, Pramesh I. Hettiarachchi, Berwyck L. Poad, Adam J. Trevitt, Gabriel da Silva, and Stephen J. Blanksby

PCCP

Physical Chemistry Chemical Physics

www.rsc.org/pccp

Volume 13 | Number 36 | 28 September 2011 | Pages 16109–16456

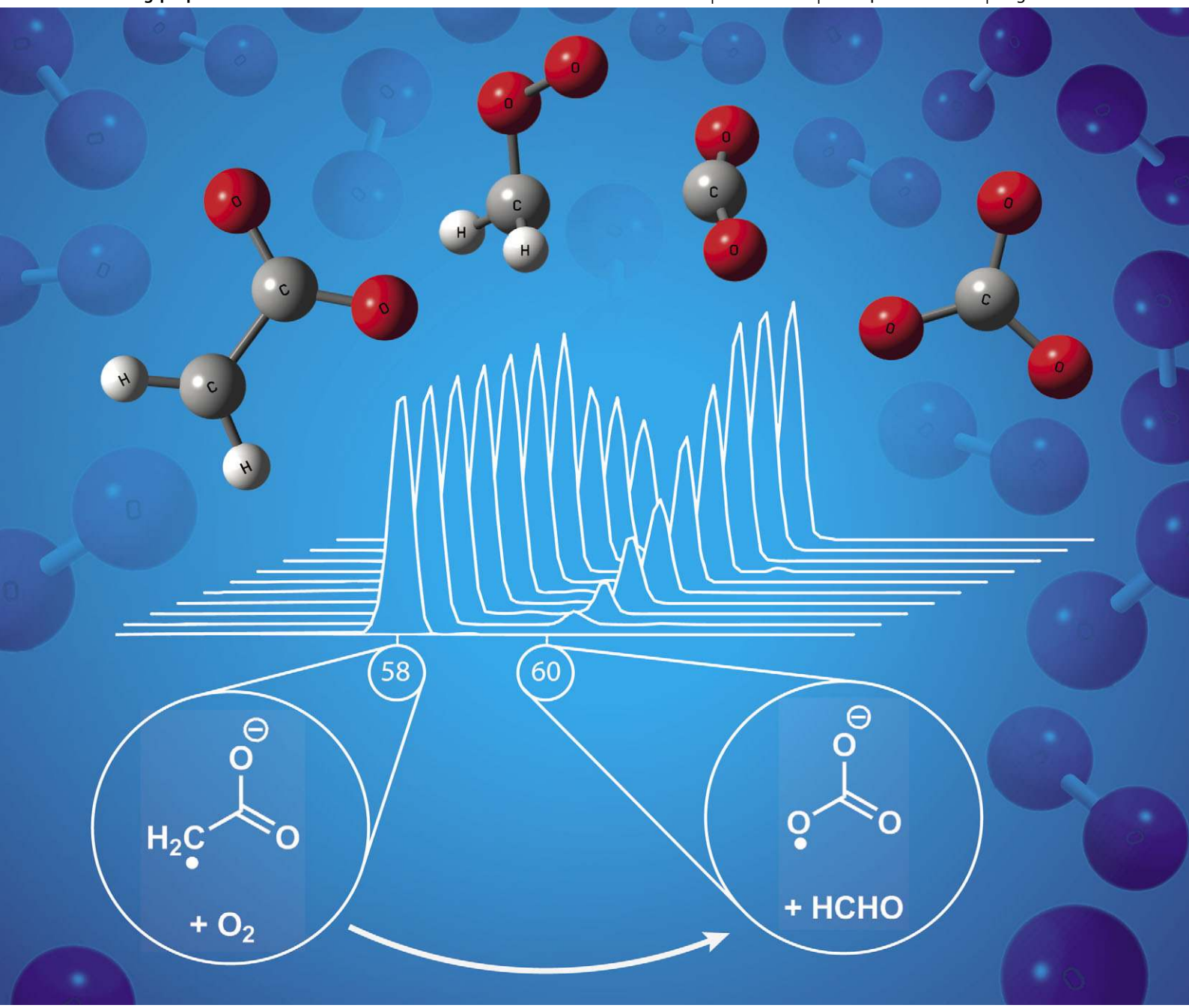

ISSN 1463-9076

COVER ARTICLE
da Silva, Blanksby *et al.*
Reactions of simple and peptidic alpha-carboxylate radical anions with dioxygen in the gas phase

HOT ARTICLE
Auinger, Mayrhofer *et al.*
Near-surface ion distribution and buffer effects during electrochemical reactions

1463-9076(2011)13:36;1-R

PCCP

Dynamic Article Links

Cite this: *Phys. Chem. Chem. Phys.*, 2011, **13**, 16314–16323

www.rsc.org/pccp

PAPER

Reactions of simple and peptidic alpha-carboxylate radical anions with dioxygen in the gas phase†

Tony Ly,‡[a] Benjamin B. Kirk,[a] Pramesh I. Hettiarachchi,[a] Berwyck L. J. Poad,§[a] Adam J. Trevitt,[a] Gabriel da Silva*[b] and Stephen J. Blanksby*[ac]

Received 16th March 2011, Accepted 22nd June 2011
DOI: 10.1039/c1cp20784a

α-Carboxylate radical anions are potential reactive intermediates in the free radical oxidation of biological molecules (*e.g.*, fatty acids, peptides and proteins). We have synthesised well-defined α-carboxylate radical anions in the gas phase by UV laser photolysis of halogenated precursors in an ion-trap mass spectrometer. Reactions of isolated acetate ($^{\bullet}CH_2CO_2^-$) and 1-carboxylatobutyl ($CH_3CH_2CH_2{}^{\bullet}CHCO_2^-$) radical anions with dioxygen yield carbonate ($CO_3^{\bullet -}$) radical anions and this chemistry is shown to be a hallmark of oxidation in simple and alkyl-substituted cross-conjugated species. Previous solution phase studies have shown that C_α-radicals in peptides, formed from free radical damage, combine with dioxygen to form peroxyl radicals that subsequently decompose into imine and keto acid products. Here, we demonstrate that a novel alternative pathway exists for two α-carboxylate C_α-radical anions: the acetylglycinate radical anion ($CH_3C(O)NH^{\bullet}CHCO_2^-$) and the model peptide radical anion, YGGFG$^{\bullet -}$. Reaction of these radical anions with dioxygen results in concerted loss of carbon dioxide and hydroxyl radical. The reaction of the acetylglycinate radical anion with dioxygen reveals a two-stage process involving a slow, followed by a fast kinetic regime. Computational modelling suggests the reversible formation of the C_α peroxyl radical facilitates proton transfer from the amide to the carboxylate group, a process reminiscent of, but distinctive from, classical proton-transfer catalysis. Interestingly, inclusion of this isomerization step in the RRKM/ME modelling of a G3SX level potential energy surface enables recapitulation of the experimentally observed two-stage kinetics.

Introduction

Carbon-centred radicals are key intermediates in numerous important chemical systems, such as those formed during tropospheric processing of volatile organics,[1] combustion of hydrocarbon fuels,[2] and free radical damage *in vivo*.[3] These radicals react rapidly with ambient molecular oxygen to produce peroxyl radicals.[4] Mass spectrometry has been widely implemented to study peroxyl radical chemistry, although in general it has been applied to the analysis of closed-shell reaction products. In some instances however, mass spectrometry has been used to synthesize charge-tagged radicals that are analogous to elusive neutral radical intermediates. These analogues, which have isolated charged and radical sites, are termed 'distonic' radical ions.[5] The distonic radical ion approach, coupled with mass spectrometry, allows for the isolation and interrogation of these reactive intermediates in the gas phase.[6]

Previous work has shown that the reaction of distonic carboxylatocyclohexyl radical anions (**1** and **2** in Scheme 1) and dioxygen results in the formation of a chemically activated peroxyl adduct that can be collisionally deactivated or can decompose through loss of $HO_2^{\bullet}$ and $HO^{\bullet}$, in good agreement with observations from studies of neutral cyclohexyl radical.[7,8] In contrast with the distonic carboxylatocyclohexyl radical anions **1** and **2**, the isomeric α-carboxylate radical ion

[a] *School of Chemistry, University of Wollongong, NSW 2522, Australia. E-mail: blanksby@uow.edu.au*
[b] *Department of Chemical and Biomolecular Engineering, The University of Melbourne, Victoria 3010, Australia. E-mail: gdasilva@unimelb.edu.au*
[c] *ARC Centre of Excellence for Free Radical Chemistry and Biotechnology, University of Wollongong, NSW 2522, Australia*

† Electronic supplementary information (ESI) available: Experimental mass spectra showing the CID of bromoacetate, the PD of iodopentanoate, the reaction of deuterium-exchanged **6** + O_2, and the synthesis of YGGFG$^{\bullet}$ and its reaction with O_2, are provided in the supporting information. Supporting theoretical evidence provided includes the full potential energy diagram calculated for acetate radical anion, concentrations of **6**, **7**, and **8** derived from the kinetic model, and coordinates, vibrational frequencies, and moments of inertia for active stationary points in the RRKM/ME calculations. See DOI: 10.1039/c1cp20784a

‡ Current Address: College of Life Sciences, University of Dundee, Dow St, Dundee DD1 5EH, UK.
§ Current Address: Department of Chemistry and Biochemistry, University of California, San Diego, USA.

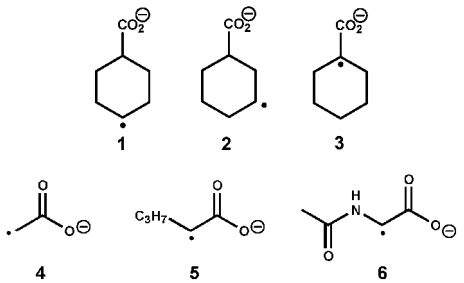

Scheme 1

(structure **3** in Scheme 1) differs significantly in chemistry, reacting with oxygen to give carbonate radical anion ($CO_3^{\bullet -}$) as the exclusive product ion, presumably *via* decomposition of a fleeting peroxyl radical intermediate through a lower energy pathway than those available to **1** and **2**.

Reaction of **3** with nitric oxide yields displacement of CO_2 by NO, which is a hallmark of cross-conjugated radical anions where the radical and the charge interact directly.[9] Given the unique chemistry of **3** towards oxygen, we were interested in using a combined experimental and theoretical approach to further study the chemistry of α-carboxylate radicals and to explore whether model biomolecular systems, based on this framework, also react with dioxygen in a similar fashion. In this study, the archetypal α-carboxylate radical anion along with model systems for α-carboxylate radicals derived from fatty acids and peptides (structures **4**, **5** and **6** respectively, Scheme 1) were synthesized by UV photodissociation of halogenated precursors in a linear ion-trap mass spectrometer.[10] Once synthesized, the radical anions were isolated in the presence of dioxygen allowing direct observation of the ionic reaction products and measurement of reaction rates.[11] We found that carbonate radical anion formation is a general feature of reactions between simple and alkyl-substituted α-carboxylate radicals (**4**, **5**) and dioxygen. Furthermore this was shown to be consistent with statistical reaction rate theory calculations based on potential energy surface derived from *ab initio* calculations. In the peptidic systems however, the amide functionality modifies the ion-molecule chemistry significantly. The reaction of dioxygen and the simple acetylglycinate radical (**6**) produces concerted loss of CO_2 and $HO^{\bullet}$ from the peroxyl adduct. Computational modelling and kinetic analysis were performed on the smaller acetylglycinate radical anion, allowing us to propose a mechanism consistent with all experimental observations. Both theory and experiment indicate that reaction occurs in two stages, namely *via* oxygen-assisted isomerization followed by further oxidation to lose CO_2 and the highly reactive $HO^{\bullet}$ radical, ultimately yielding a smaller diamide. Interestingly, the same dissociation chemistry is also observed for α-carboxylate radicals derived from a larger peptide, *i.e.*, $YGGFG^{\bullet -}$.

Experimental methods

Materials

Methanol (HPLC grade), acetic anhydride, and ammonia solution (28%) were obtained from Ajax (Sydney, Australia). $^{18}O_2$ gas (95%) was obtained from Cambridge Isotope Laboratories (Andover, MA). Bromoacetic acid, chloramine T trihydrate, sodium iodide (anhydrous), leucine enkephalin peptide (YGGFL), 2-bromopentanoic acid, and sodium metabisulfite were purchased from Sigma-Aldrich (St. Louis, MO). L-Tyrosine was purchased from BDH Lab Supplies (now part of VWR International, West Chester, PA). All commercial compounds were used without further purification. 2-Iodopentanoic acid was prepared from 2-bromopentanoic acid by a standard procedure.[12,13] Water was purified to 18.2 MΩ resistivity using a Millipore (Billerica, MA) Synergy UV water purification system.

Mass spectrometry

Methanolic solutions of analytes were prepared at 10–50 μM concentrations and infused at a rate of 3–5 μL/min into the electrospray ionisation source of a ThermoFisher (San Jose, CA) LTQ linear quadrupole ion-trap mass spectrometer. The LTQ was modified to perform both photodissociation and ion-molecule reactions in the ion trap (see below for details). Aqueous ammonia was added to raise the pH when required to facilitate the dianion formation. Typical source parameters were spray voltage −2.5 and +3.5 kV (for negative and positive ion mode, respectively), capillary temperature 200–250 °C, sheath gas flow between 10 and 30 (arbitrary units), and sweep and auxiliary gas flow set at between 0 and 10 (arbitrary units). For collision experiments, ions were mass-selected with a window of 1–4 m/z and fragmented using default instrument parameters, *i.e.* 0.250 activation q-parameter, 30 ms activation time (unless otherwise noted) and normalized collision energies of 20–40 (arbitrary units).

Photodissociation

The linear ion-trap mass spectrometer is modified in a similar fashion to previously described.[10,14] A 2.75 in. quartz viewport (MDC Vacuum Products, Hayward, CA) is affixed to the posterior plate of the spectrometer vacuum housing with a CF flange to allow transmission of 266 nm laser pulses from a flashlamp-pumped Nd:YAG laser (Continuum, Santa Clara, CA). The laser beam is directed into the trap *via* two right-angle prisms, which are adjusted to optimize overlap with the ion cloud. The laser energy is *ca.* 2 mJ/pulse, unfocussed, contained within a 3 mm spot diameter and 5 ns pulse duration. A single laser pulse irradiates trapped ions at a time synchronized to the beginning of the activation step of a typical MS^n experiment by feeding a differential signal from the instrument to the laser flashlamp trigger *via* a digital delay generator (Berkeley Nucleonics, San Rafael, CA). The MS stage that is synchronized with the pulsing of the laser can be chosen using the Diagnostics menu of the default instrument tuning software. The photodissociation efficiencies achieved are comparable to previously reported,[10,15] *e.g.*, the yield of iodine atom loss is ~20% for iodoYGGFL (see Supporting Information Fig. S1†).

Ion-molecule reactions

Modifications to the linear ion-trap mass spectrometer to allow the introduction of neutral gases into the ion trap region of the instrument have been described previously.[11]

Briefly, gas reagents in a syringe are introduced into a flow of Ultra High Purity (UHP) helium (3–5 psi) *via* a heated septum inlet (25–250 °C). The gas mixture is introduced into the ion trap *via* a variable leak valve, which is adjusted until the ion gauge reads $\sim 0.9 \times 10^{-5}$ Torr, which indicates an ion trap pressure of ~ 2.5 mTorr. The temperature of the vacuum manifold surrounding the ion trap was measured at 307 ± 1 K, which is taken as being the effective temperature for ion-molecule reactions observed therein.[16] Reaction times of 30–10 000 ms were set using the activation time parameter within the control software using no collision energy applied. All spectra presented are an average of at least 50 scans. The concentration of dioxygen in the ion trap was measured using a calibrant reaction where the true second order rate constant is known (carboxylatoadamantyl radical anion + O_2): thus, the $[O_2]$ is simply $k_{\text{pseudo first order}}/k_{\text{second order}}$. Rate coefficients were determined as previously described with an estimated measurement accuracy of ±25%.[11] Collision rates for the ion-molecule reactions were estimated by the parameterized trajectory collision theory of Su and Chesnavich[17] and branching ratios were calculated using the method of Grabowski and Zhang.[18]

Theoretical methods

Quantum chemical calculations

Electronic structure theory calculations are performed in Gaussian 09.[19] The B3LYP/6-31G(2df,p) model chemistry is used to optimize structures and calculate vibrational frequencies. The high-level G3SX composite theoretical method is used for molecular energies.[20] The G3SX method uses B3LYP/6-31G(2df,p) optimized geometries and zero point energies along with higher-level wavefunction theory single point energies from HF through QCISD(T) theory, with basis sets of incrementally decreasing size. These energies are combined with empirical scaling corrections to arrive at the final G3SX energy. The G3SX method is particularly accurate for barrier heights (relative to computational expense),[21] and also performs well for a range of thermochemical properties.[19] The G3SX enthalpies reported in this study are expected to be accurate to ±1.5 kcal/mol (95% confidence intervals).[20,21]

Reaction rate calculations

Reaction yields and apparent rate constants, $k(T,P)$, for chemically activated reaction of both the acetate (**4**) and acetylglycinate (**6**) radical anions with O_2 are obtained from stochastic solutions of the 1D Master Equation (ME), using MultiWell-2010.1.[22] Densities and sums of states are determined from Stein-Rabinovitch-Beyer-Swinehart counts, based on B3LYP/6-31G(2df,p) vibrational frequencies and moments of inertia. Internal degrees of freedom are treated as harmonic-oscillators, with external degrees of freedom modeled as an active 1D and an inactive 2D rotor, following the conventional assumption of a symmetric top. Rice-Ramsperger-Kassel-Marcus (RRKM) theory is used for microcanonical $k(E)$, with the inclusion of tunneling corrections for H-shift reactions *via* an Eckart barrier. Collisional energy transfer is described using a single exponential-down model with a constant ΔE_{down} value of 600 cm^{-1}. A grain size of 10 cm^{-1} is used for the energy-grained component of the hybrid master equation, for energies up to 30 000 cm^{-1}. The continuum component of the master equation is then solved up to 200 000 cm^{-1} across a further 6000 grains. Barrierless reactions are described using the hindered Gorin transition state model,[23] with the high-pressure limit rate constant set to that calculated by collision theory. Reported RRKM/ME simulations represent ten million trials of 200 collisions each. Calculations were performed at 307 K and 2.5 mTorr of He. Coordinates for optimized structures, vibrational frequencies, and moments of inertia for all active species and transition states involved in the RRKM/ME calculations are provided as Supporting Information.

Results and discussion

The acetate radical anion (**4**) is an archetypal cross-conjugated radical anion,[9] which is conveniently synthesized *in vacuo* by UV photolysis of the C–Br bond in bromoacetate ($BrCH_2CO_2^-$). Electrospray ionisation (ESI) of a methanolic solution of bromoacetic acid yields the two naturally occurring isotopologues of the bromoacetate anion at m/z 137 and 139. Isolation of these ions in the ion trap and photodissociation (PD) *via* irradiation with a single pulse of 266 nm photons from an Nd : YAG laser yields the target radical anion **4** at m/z 58 along with bromide anions at m/z 79 and 81 (Fig. 1a). In contrast, conventional collision induced dissociation (CID) of bromoacetate yields bromide as the exclusive product ion (see Supporting Information Fig. S2). As observed previously for the α-carboxylate cyclohexyl radical (**3**), reaction of **4** and dioxygen yields carbonate radical anion at m/z 60, which increases in abundance with increasing reaction time, as shown in Fig. 1b. Reaction of **4** with $^{18}O_2$ produces a 2 Th mass shift in the product ion, indicating incorporation of one atom from dioxygen, as shown in Fig. 1c. A plot of the natural log of the fractional precursor intensity *versus* time is well-described by a linear fit ($R^2 = 0.992$), indicating that the reaction conditions are pseudo first-order (see Supporting Information Fig. S3). A second order rate constant of 7.5×10^{-11} cm^3 $molecule^{-1}$ s^{-1} is obtained using the pseudo first-order rate constant and the concentration of O_2 in the trap (7.1×10^9 molecule cm^{-3}), which is determined using a calibrant ion-molecule reaction.[11] A calculated reaction efficiency of $\sim 12\%$ is derived from the measured second order rate constant and the predicted collision frequency, which is 6.5×10^{-10} cm^3 $molecule^{-1}$ s^{-1}. The reaction efficiency is relatively high, and is comparable to rates determined for the reactions of distonic radicals with molecular oxygen.[7,11]

While PD of 2-bromopentanoate produced a very low abundance of the desired radical anion, the 2-iodopentanoate anion (m/z 227) gave rise to a moderate abundance of **5** at m/z 100 (see Supporting Information Fig. S4). By analogy with bromoacetate (Fig. 1a), PD of the 2-iodopentanoate anion also yields the halide anion (in this case iodide at m/z 127) as a major competing pathway. Interestingly, the extension of the alkyl chain presents two additional competitive channels *via* β-scission of the nascent radical yielding m/z 99 ($-H^\bullet$) and m/z 71 ($-CH_3CH_2^\bullet$). These processes presumably occur over a

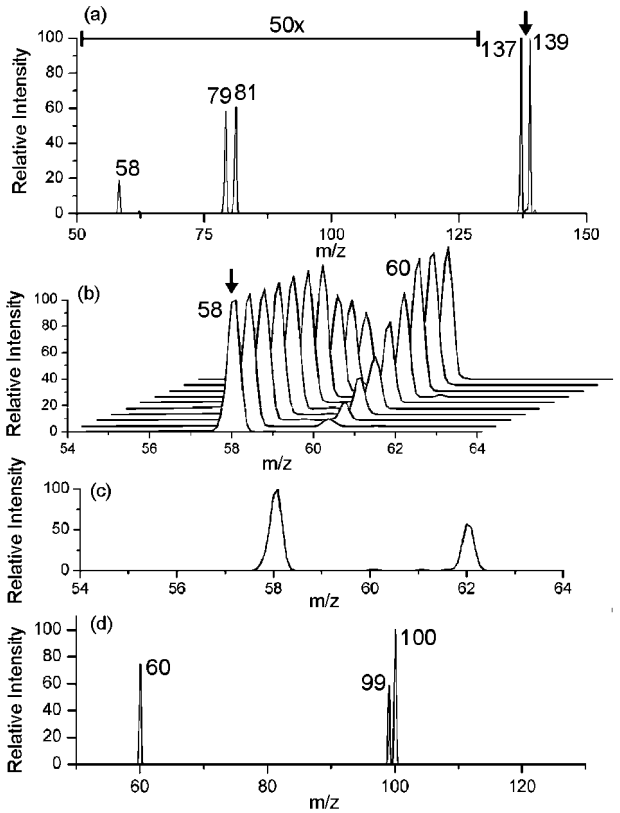

Fig. 1 (a) Irradiation of bromoacetate ($BrCH_2CO_2^-$) cleaves the carbon-bromine bond to produce acetate radical anion (**1**) at *m*/*z* 58. (b) Reaction of isolated **1** with molecular oxygen for the following reaction times (in ms), bottom to top: 30, 200, 400, 600, 800, 1000, 1200, 1500, 1700, and 2000 yields the carbonate radical anion at *m*/*z* 60. (c) The corresponding reaction with $^{18}O_2$ yields a carbonate radical anion that is 2 mass-units heavier, indicating incorporation of one oxygen atom from molecular oxygen. (d) Isolation of the 1-carboxylatobutyl radical anion (**5**) at *m*/*z* 100 in the presence of dioxygen and allowed to react for 4000 ms. The ion at *m*/*z* 99 forms from *m*/*z* 100 during isolation of the latter and is unreactive toward O_2 (see text).

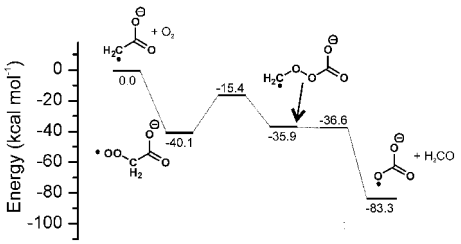

Fig. 2 Calculated energy surface for reaction of acetate radical ion (**4**) with O_2. Energies represent relative 298 K enthalpies calculated at the G3SX level of theory, in kcal mol^{-1}.

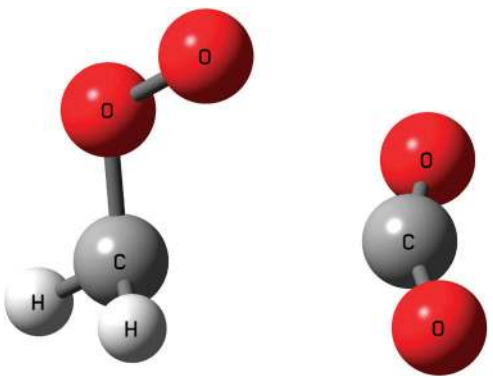

Fig. 3 Optimized structure for the transition state corresponding to isomerization of the peroxyl radical formed in the acetate radical ion (**4**) + O_2 reaction (B3LYP/6-31G(2df,p) level). The transition state structure illustrates concerted C–C bond scission and C–O bond formation.

low barrier and as a consequence it was found that the target radical anion **5** at *m*/*z* 100 could not be isolated in the absence of *m*/*z* 99 (Fig. 1d). Nevertheless the ion abundance of the closed-shell species *m*/*z* 99 was found to be unaffected by increasing the reaction time in the presence of dioxygen and as such can be considered a spectator to its radical companion at *m*/*z* 100. The radical anion **5** at *m*/*z* 100 was found to yield the carbonate radical anion at *m*/*z* 60 as the exclusive ionic product of the reaction with dioxygen (Fig. 1d) consistent with the archetypal α-carbonate radical **4** (Fig. 1b) and the previously investigated 1-carboxylatocyclohexyl radical **3**.[7]

The calculated energy surface for the reaction of **4** and dioxygen is shown in Fig. 2. Addition of O_2 is around 40 kcal mol^{-1} exothermic, which is typical of O_2 association with an alkyl radical. The **4** + O_2 reaction yields a peroxyl radical that undergoes an *ipso* rearrangement to form methyl carbonoperoxoate radical anion, *via* the transition state structure depicted in Fig. 3. *β*-Scission from the α-peroxide radical takes place with a negligible barrier, and leads to formaldehyde and carbonate radical anion. The barriers to these unimolecular rearrangements are modest, and remain lower than the entrance channel. The observed carbonate radical is consistent with the mechanism presented in Fig. 2, which also accurately predicts that one of the oxygen atoms in carbonate radical originates from molecular oxygen. Interestingly, hydrogen carbonate and formyl radical are predicted to be the most thermodynamically favorable products on the $C_2H_2O_4$ energy surface (*i.e.*, 89.6 kcal mol^{-1} below **4** + O_2 at the G3SX level; see Supporting Information Figure S5). It may be possible for these products to form *via* a roaming radical mechanism in the formaldehyde–carbonate radical anion complex before dissociation to the observed products, although the experiments reported here provide no evidence for this taking place.

The **4** + O_2 reaction has been simulated with RRKM/ME theory, according to the mechanism depicted in Fig. 2. Because the barrier for *β*-scission of the peroxide intermediate is predicted to fall below the radical energy, this step is neglected in these calculations, and we assume instead that the *ipso* rearrangement transition state leads directly to formaldehyde + carbonate radical. The RRKM/ME simulations (see Methods: Reaction Rate Calculations) predict that the formaldehyde + carbonate radical products account for 8.6% of the reaction yield, with the remainder corresponding to reverse reaction back to **4** + O_2. This compares favorably to the experimentally determined efficiency of 12%, given the expected uncertainties in the theoretical calculations, the collision theory rate constant, and difficulties in quantifying the accuracy of the experimental measurements.

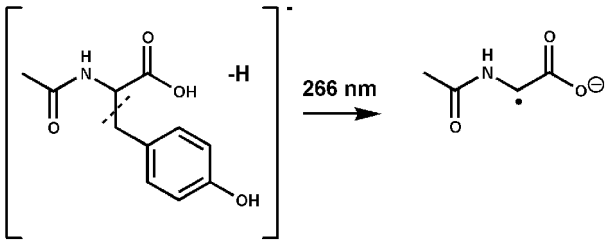

Scheme 2

We sought to investigate whether similar chemistry is observed for peptidic α-carboxylate radical anions. Potential peptidic sites for α-carboxylate radicals include the C_β of aspartate, the C_γ of glutamate, and the C_α of any non-amidated C-terminal residue. Radical acetylglycinate (**6**) was chosen as a model system for a peptidic C-terminal C_α-centred radical. As in **4** and **5**, the radical in **6** interacts with the charge. However, the amide group provides an additional lone pair that can conjugate with the radical and thus modify the ion-molecule chemistry. Previous work has suggested that protonated glycine radical can be prepared from UV photodissociation of tyrosine *via* neutral loss of 107 Da.[24]

We predicted that similar UV photodissociation chemistry could be leveraged to synthesize **6**, as shown in Scheme 2. The mass spectrum resulting from irradiation of deprotonated *N*-acetyltyrosine at 266 nm (Fig. 4a) shows numerous photodissociation products including neutral loss of 107 Da, presumably through cleavage of the C_α–C_β bond to form **6**. In contrast to both **4** and **5**, reaction of isolated **6** with dioxygen does not result in formation of the carbonate radical

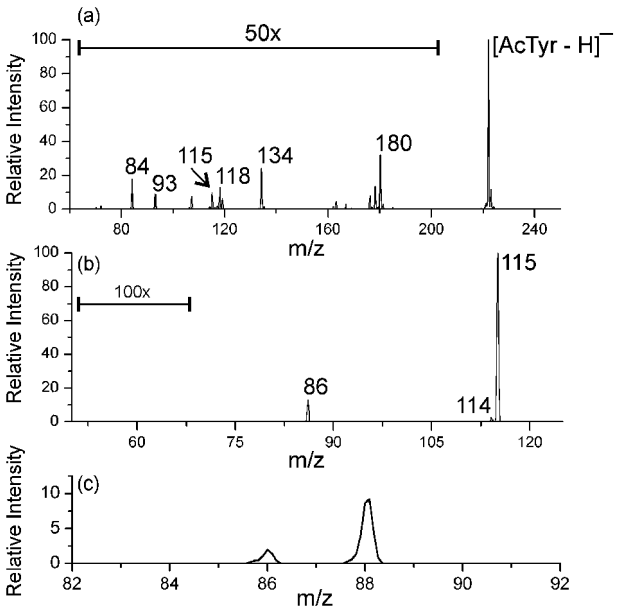

Fig. 4 (a) PD spectrum of acetyltyrosinate anion. (b) Reaction of the acetylglycinate radical anion (**6**) with molecular oxygen for 1 s yields the product ion at *m*/*z* 86, which is due to addition of molecular oxygen, followed by concerted loss of CO_2 and HO•. A very minor −1 Da product observed at *m*/*z* 114, which is not present during isolation, is likely due to $+O_2$, followed by $-HO_2$•. (c) Reaction with $^{18}O_2$ produces a 2 Th shift to form *m*/*z* 88 with the low abundance *m*/*z* 86 arising from residual $^{16}O_2$.

anion at *m*/*z* 60 but rather a neutral loss of 29 Da (*i.e.*, *m*/*z* 86 in Fig. 4b). The analogous reaction with $^{18}O_2$ shifts the product mass-to-charge ratio by 2 Th (Fig. 4c) indicating the transfer of a single oxygen atom. While substitution of the amide hydrogen with a deuterium does not change the product mass, suggesting that the amide hydrogen is lost to form *m*/*z* 86 (see Supporting Information Fig. S6). It is proposed that this product ion arises from addition of O_2 to **6**, followed by concerted loss of CO_2 and HO• and this interpretation is supported by theoretical modelling of the potential energy surface as discussed below. Unlike the **4** + O_2 reaction, a plot of the natural log of the fractional precursor intensities *versus* time is notably non-linear, indicating more complex reaction dynamics, as explained below.

The energy surface developed for the **6** + O_2 reaction is illustrated in Fig. 5. Initial association of the radical anion with O_2 forms a peroxyl radical intermediate, although in this case the exothermicity is reduced considerably from that calculated for **4** + O_2 (−32.9 kcal mol^{-1} compared with −40.1 kcal mol^{-1} for the latter). This is due to conjugation between the amide group and the radical site that is lost upon O_2 addition. Despite this, we still identify four transition states resulting in transformation of the peroxyl radical that occur with energy below the entrance channel. The highest-energy pathway is for HO_2• elimination, which forms a hydrogen-bonded complex involving the imine and the HO_2• radical. The isomerization occurs at 1.7 kcal mol^{-1} below the energy of the reactants and the dissociated products are actually 3.8 kcal mol^{-1} above the reactants. Formation of an imine and the hydroperoxyl radical is considered the dominant pathway in the oxidation of peptide radicals,[25] and we do detect evidence for this reaction as a very minor channel in the **6** + O_2 process (*i.e.*, *m*/*z* 114 in Fig. 4b). The pathway with the next lowest energy is for formation of carbonate radical anion plus a neutral carbonyl compound (*N*-formyl-acetamide), which occurs at 6.4 kcal mol^{-1} below the entrance channel. This reaction takes place *via* a transition state of similar structure to that depicted in Fig. 3 for the analogous process in acetate radical ion oxidation. The barrier for isomerization of the peroxyl radical (26.5 kcal mol^{-1} with respect to the peroxyl radical) is also similar to that found for the corresponding process in the **4** + O_2 mechanism (24.7 kcal mol^{-1}). Despite this pathway requiring a somewhat smaller barrier than the imine + HO_2• channel, no experimental evidence is detected for carbonate radical formation (*i.e.*, *m*/*z* 60 is not observed in Fig. 4b).

The **6** + O_2 mechanism reveals a transition state lower yet in energy, leading directly from the peroxyl radical to the hydroxyl radical, CO_2, and an anionic carbonyl species (*N*-formylacetamide anion, **8**). The transition state structure for this dissociation reaction is depicted in Fig. 6, where we observe that it involves a concerted intramolecular hydrogen shift and C–CO_2 bond scission. Intrinsic reaction coordinate scans demonstrate that initial fragmentation to CO_2 and $CH_3C(O)N^-C^•(H)OOH$ is followed by *β*-scission to HO• and **8**, without any further barrier. This transition state lies 15.1 kcal mol^{-1} below the reactant energies, with barrier of only 17.8 kcal mol^{-1} relative to the peroxyl radical. Loss of HO• and CO_2 from the anion **6** upon O_2 addition *via* this

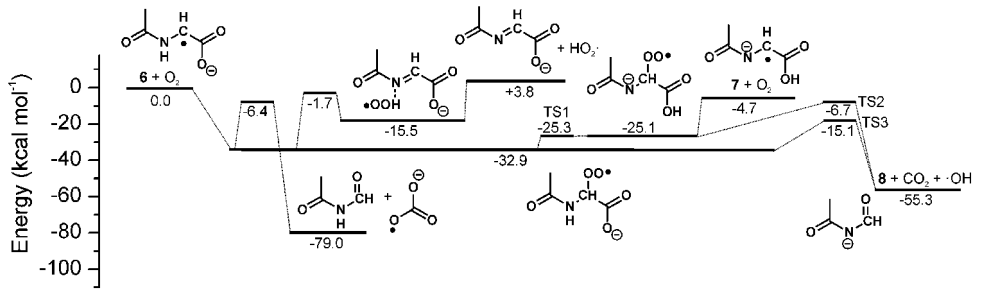

Fig. 5 Calculated energy surface for reaction of acetylglycinate radical ion (**6**) with O_2. Energies represent relative 298 K enthalpies calculated at the G3SX level of theory, in kcal mol^{-1}.

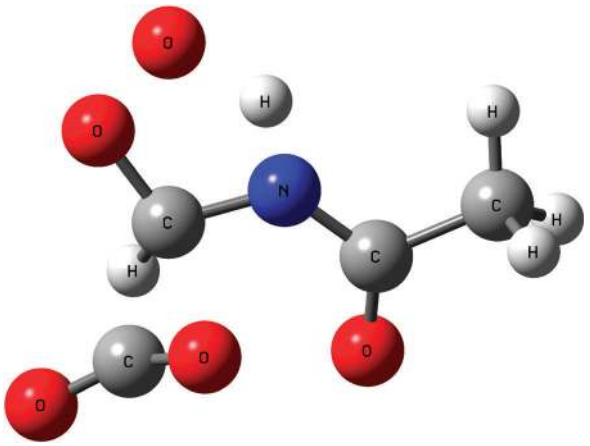

Fig. 6 Optimized structure for the transition state corresponding to CO_2, HO$^\bullet$ loss from the peroxyl radical formed in the acetylglycinate radical anion (**6**) + O_2 reaction (B3LYP/6-31G(2df,p) level). This transition state structure illustrates concerted hydrogen shift and C–C bond scission.

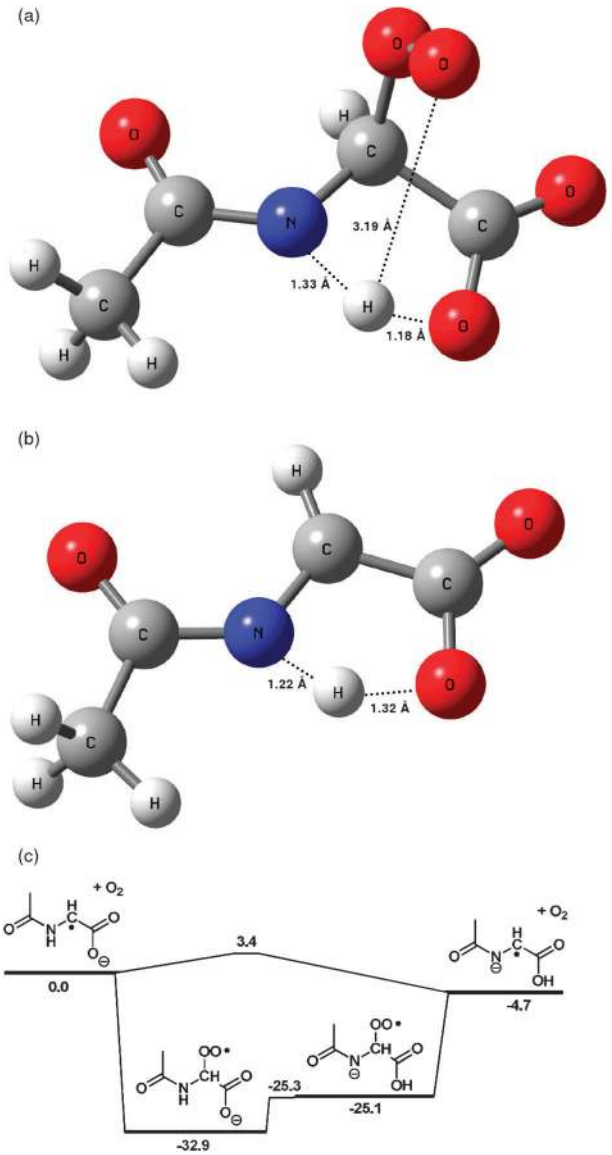

Fig. 7 (a) Optimized structure for the transition state corresponding to isomerization of the peroxyl radical formed in the acetylglycinate radical anion (**6**) + O_2 reaction. (b) Optimized structure for direct intramolecular proton transfer connecting radical anions **6** and **7** (B3LYP/6-31G(2df,p) level). (c) Reaction energetics for direct proton transfer compared with that facilitated by reversible oxygen addition. Energies represent relative 298 K enthalpies calculated at the G3SX level of theory, in kcal mol^{-1}.

mechanism is responsible for the dominant product ion signal observed at m/z 86 (Fig. 4b). The mechanism identified for the formation of these products is also consistent with the isotope labeling experiments, which indicated loss of the amide hydrogen and incorporation of one oxygen atom from O_2 in the product ion. The fact that the carbonate radical is not detected in acetylglycinate radical anion oxidation, whereas it is the dominant acetate radical anion oxidation product, supports our theoretical prediction that the former radical possesses much lower-energy reaction pathways in its reaction with molecular oxygen.

The results described above explain the observed reaction products from **6** + O_2, but do not explain the multi-step reaction kinetics measured in these experiments. We find that this behavior can be explained by a novel oxygen-assisted isomerization. Fig. 5 illustrates that the **6** + O_2 reaction forms a peroxyl radical for which the lowest-energy transition state corresponds to proton transfer from the amide nitrogen to a carboxylate oxygen resulting in the slightly more energetic (+7.6 kcal mol^{-1}) amide-centred anion. The structure of this transition state is shown in Fig. 7(a) and reveals that the migrating proton is closer to the carboxylate oxygen (1.18 Å) than the amide nitrogen (1.33 Å). For comparison, Fig. 7(b) shows the equivalent transition state for direct, unassisted unimolecular conversion of **6** to **7** and reveals the migrating

Table 1 Rate constants for reaction of the radical ions **4**, **6**, and **7** with dioxygen

Reaction	k (cm^3 molecule^{-1} s^{-1})	
	Experimental	Theoretical[a]
4 + O_2 → HCHO + $CO_3^{\bullet -}$ (k_1)	7.51×10^{-11}	5.54×10^{-11}
6 + O_2 → **7** + O_2 (k_2)	1.52×10^{-10}[b]	4.13×10^{-10}
6 + O_2 → **8** + CO_2 + HO$^\bullet$ (k_3)	–[b]	1.76×10^{-10}
7 + O_2 → **8** + CO_2 + HO$^\bullet$ (k_4)	1.52×10^{-10}[b]	4.25×10^{-10}

[a] From RRKM/ME simulations. [b] Determined from a least-squares fit assuming a two-step (k_2, k_4) reaction mechanism.

proton closer to the carboxylate oxygen (1.22 Å) than the amide nitrogen (1.32 Å). This geometry suggests an earlier transition state consistent with this slightly exothermic isomerization (−4.7 kcal mol^{-1}). A comparison of the energetics of direct proton transfer to that facilitated by formation of intermediate peroxyl radicals is shown in Fig. 7(c) and illustrates the net reduction in the reaction barrier from +3.4 to −25.3 kcal mol^{-1} afforded by participation of the dioxygen molecule. This dramatic lowering of the barrier is reminiscent of classical "proton transfer catalysis" where the transition state energies for intramolecular proton transfer within an ion are lowered by partial solvation of the proton by a neutral atom or molecule.[26,27] There are however three distinctive features of the effect observed here: (i) the neutral molecule is covalently attached to the ion in the transition state, *i.e.*, the dioxygen in this instance is present as a formal peroxyl moiety in the transition state; (ii) the proton transfer is remote from the peroxyl moiety by some 3.19 Å and; (iii) while there is a net lowering in transition state energy due to addition of the oxygen, the barrier for the proton transfer relative to the peroxyl radical is actually higher (+7.8 kcal mol^{-1})[28] than that for the unassisted pathway (+3.4 kcal mol^{-1}). The absence of even a partial bonding or solvation interaction between the neutral "catalyst" and the transferring proton in the transition state is distinct from classical proton-transfer catalysis. It appears that the catalytic role of the oxygen in the present system is simply to provide the necessary energy (−32.9 kcal mol^{-1}) to fuel the proton transfer reaction *via* reversible formation of the peroxyl radical. While the reversible addition of dioxygen to carbon-centred radicals is well-known from solution phase studies,[29] the indirect proton transfer catalysis observed here is likely to be unique to the gas phase where the excess energy from formation of the new C–OO bond remains with the system and can be used to power the isomerization.

Calculations reveal that isomerization of the intermediate peroxyl radical anion can result in formation of a rearranged radical anion **7** by loss of O_2 but, in addition, the intermediate can undergo competitive loss of CO_2 + HO$^\bullet$ (Fig. 5). The latter pathway is actually somewhat lower in energy (−6.7 kcal mol^{-1} below the entrance channel) but will be less favored in terms of entropy than the direct dissociation. Because **6** and **7** are isobaric, the mass spectrometry experiments do not allow for direct differentiation of these products, nor can they exclude the possibility of direct rearrangement of **6** to **7** over the relatively modest barrier of +3.4 kcal mol^{-1}. Through analysis of the kinetics however, we show that the involvement of the oxygen-assisted isomerization pathway provides a more satisfactory explanation for the measured reaction kinetics (see below).

Reaction rate simulations have been performed for both **6** + O_2 and **7** + O_2, in both cases incorporating all pathways depicted in Fig. 5. Rate constants for the radical ion + O_2 steps were determined to be 5.89×10^{-10} cm^3 molecule^{-1} s^{-1} from trajectory collision theory, whereas dissociation of the imine–$HO_2^\bullet$ complex was treated with the reverse reaction having a rate constant of 1×10^{-11} cm^3 molecule^{-1} s^{-1}, consistent with variational transition state theory calculations on dissociation of similar $HO_2^\bullet$ radical complexes.[30,31] The **6** + O_2 reaction is predicted to yield 70.1% **7** + O_2 and 29.8% **8** + CO_2 + HO$^\bullet$, with 0.1% **6** + O_2 *via* the reverse reaction. The carbonate radical anion and $HO_2^\bullet$ radical pathways were predicted to take place to only a minor extent (respective yields of 0.004% and 0.00001%). For the **7** + O_2 reaction, the dominant products are **8** + CO_2 + HO$^\bullet$ (72.1%), with a significant null reaction channel reforming **7** + O_2 (27.9%). Minor amounts of **6** + O_2 (0.005%) and carbonate radical + *N*-formyl-acetamide (0.001%) are also predicted to form, whereas the branching ratio to the $HO_2^\bullet$ channel is too low to calculate.

Calculated rate constants for the formation of important products in reactions of **6** and **7** with O_2 are listed in Table 1. These rate constants have been used to model the oxidation kinetics of acetylglycinate in the ion trap. Consistent with the experimental settings, we assumed that all concentrations were homogeneous and that O_2 was in significant excess, with the total constant [O_2] concentration at 7.1×10^9 molecule cm^{-3}. The set of simultaneous ordinary differential equations (ODEs) describing [**6**], [**7**], and [**8**] were then solved numerically, using previously-developed code.[32] The resultant concentrations, normalized to unity initial reactant concentration, are provided as Supporting Information (Fig. S7), compared to experimental fractional intensities for m/z = 115 (**6** + **7**) and 86 (**8**). The calculated rate constants result in an apparent reaction rate faster than that observed experimentally, although they do manage to describe the two-stage kinetics. Here, the slow initial reaction rate can be attributed to oxygen-assisted isomerization of **6** to **7**, with the apparent rate of reaction subsequently increasing due to the faster **7** + O_2 reaction to form **8** + CO_2 + HO$^\bullet$.

In order to further investigate the complex kinetics observed for the **6** + O_2 reaction in the ion trap we attempted to numerically fit experimental values to k_2–k_4. Initial trials revealed that the results could be adequately described using only k_2 and k_4, implying the mechanism **6** + O_2 → **7** + O_2 → **8** + CO_2 + HO$^\bullet$. The closed-form solution to the reduced system of ODEs describing [**6**] and [**7**] (where [**8**] = 1–[**6**]–[**7**]) as a function of time was obtained using the inverse Laplace transform method (with unity initial reactant concentration).[33] A least-squares procedure was then used to obtain best fits to k_2 and k_4, which for both rate constants provided values of 1.52×10^{-10} cm^3 molecule^{-1} s^{-1}. Fig. 8 demonstrates that the fitted two-step mechanism accurately reproduces the observed kinetics. Reasonable fits can still be obtained using small values of k_3 (on the order of 10^{-11} cm^3 molecule^{-1} s^{-1}), although no value for this rate constant improved the agreement

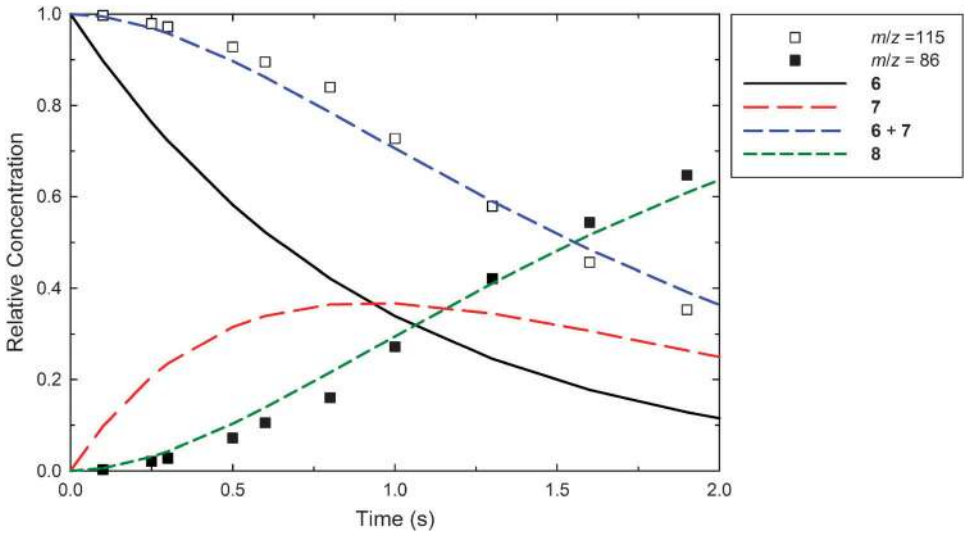

Fig. 8 Kinetics of the acetylglycinate radical ion (**6**) + O_2 reaction. Dot points represent experimental results (relative ion intensities). Solid lines represent least-squares fit of the experimental data assuming the mechanism **6** + O_2 → **7** + O_2 → **8** + CO_2 + $HO^{\bullet}$.

between model and experiment. The experimental rate constants for **6** + O_2 and **7** + O_2 correspond to a reaction efficiency of 26%, comparable to the value determined for **4** + O_2 (12%) and, as noted, comparable to literature values for other radical ion reactions with O_2.[7,11] The experimental rate constants are in relatively good agreement with the purely theoretical RRKM/ME values, which are too large by around a factor of two. The reported acetylglycinate radical ion + O_2 experiments, and accompanying theoretical and kinetic analysis, therefore provide evidence for two novel low-energy reactions, one that achieves oxygen-assisted isomerization of the reactant and another that results in formation of the highly reactive hydroxyl free radical.

A peptide was examined next to determine whether the ion-molecule chemistry observed for **6** would extrapolate to larger systems. It has been previously shown that radical peptides can be synthesized from iodinated peptide precursors.[34] Here, the tyrosine residue of YGGFL was iodinated using published procedures and then acetylated to block deprotonation of the tyrosine sidechain, thus favouring a charged C-terminus. PD of the peptide derivative cleaves the carbon-iodine bond, yielding a radical at the tyrosine sidechain (see Supporting Information Fig. S8a). CID of the peptide radical produces sidechain losses, predominantly from leucine, and backbone fragmentation.[15] Previous studies have shown that sidechain losses and backbone fragmentation are due to radical migration (via hydrogen atom abstraction), followed by β-scission. In the case of the 56 Da loss, β-scission occurs from a Leu C_γ radical, effectively transforming Leu to a C_α-radical Gly, *i.e.*, an alpha carboxylate radical, as shown in Scheme 3. Reaction of $YGGFG^{\bullet -}$ with dioxygen yields loss of 29 Da (Scheme 3), which is the same loss observed for **6** (see Supporting Information Fig. S8b). The loss of 29 Da is not observed in the CID of $YGGFG^{\bullet -}$ (see Supporting Information Fig. S8c), confirming that the product is a result of specific ion-molecule chemistry and not simply dissociation of a metastable precursor. These results indicate that a general feature of reactions between peptidic α-carboxylate radical anions and oxygen is the production of hydroxyl radicals with concomitant expulsion of carbon dioxide.

Peptidic C_α radicals are predicted to form as a result of free radical damage *in vivo*. These radicals are highly stabilized by captodative interactions from the neighbouring amide and carbonyl groups.[35,36] However, pulse radiolysis experiments on model amino acids have shown that these radicals react quickly with oxygen to produce peroxyl radical intermediates that undergo backbone scission to form an amide and an α keto acid.[25] Further experiments demonstrated that other species such as pyruvic acid, acetaldehyde, acetic acid, and carbon dioxide are also produced in significant yields.[37] Intermolecular recombination of two amino acid peroxyl radicals was proposed as a possible explanation for these side-products. In this manuscript, we show that a novel unimolecular dissociation pathway is available to α-carboxylate peroxyl radicals isolated in the gas phase, namely loss of carbon dioxide and generation of hydroxyl radical. This **8** + CO_2 + $HO^{\bullet}$ pathway is, however, likely to be competitive with the imine + keto acid pathway (*cf.* Scheme 4) even in aqueous solution, due to the low barrier heights relative to the peroxyl radical (Fig. 5). Indeed, the observation of carbon dioxide in gamma-irradiated amino acids and peptides is entirely consistent with the novel pathway described here.

Conclusions

We have explored the gas phase ion-molecule reactions of oxygen and cross-conjugated radical anions, including model and larger biomolecular systems. The archetypal cross-conjugated radical anion, the acetate radical anion (**4**), reacts with oxygen to produce carbonate radical anion exclusively. The reactivity observed is completely consistent with the 1-carboxylatocyclohexyl radical (**3**) examined previously.[7] The reactivity of the 1-carboxylatobutyl radical anion (**5**) is diminished somewhat, but carbonate radical remains a significant product. Combined, these results indicate that the carbonate radical anion formation is a general feature in the

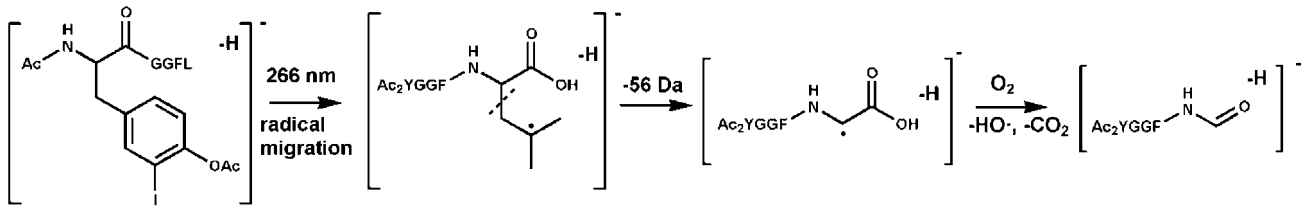

Scheme 3

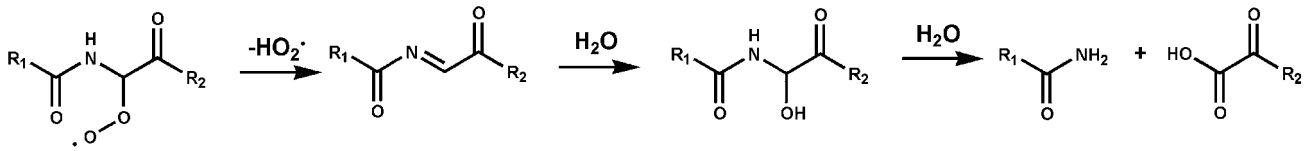

Scheme 4

reactions of simple and alkyl-substituted α-carboxylate radical anions with oxygen. Furthermore, the efficiency and selectivity of this reaction suggests that this product ion at m/z 60 may be used as a diagnostic ion for the presence of cross-conjugated radical anions. Indeed, the clear distinction in reactivity between the radical anion **3** and its distonic isomers **1** and **2** suggests that the term distonoid radical ions—coined by Eberlin and co-workers[38]—may be usefully applied to the former system as well as the other α-carboxlyate radical anions studied here (**4**, **5** and **6**).

We demonstrate that the ion-molecule chemistry changes significantly when the α-carboxylate radical anion motif is incorporated into amino acids and peptides. In such instances, the presence of the neighbouring amide functionality enables access to new pathways that are significantly lower in energy than carbonate radical anion formation. In the archetypal peptidic system, acetylglycinate radical anion (**6**), the concerted loss of carbon dioxide and hydroxyl radical is the dominant pathway observed. Similar ion-molecule chemistry is observed in a larger peptidic α-carboxylate radical anion. Interestingly, the kinetics measured for the acetylglycinate + O_2 reaction had significant curvature, consisting of a "slow" followed by a "fast" component. Theoretical calculations point to a novel oxygen-assisted isomerization whereby reversible formation of a peroxyl moiety facilitates proton transfer from the amide to the carboxylate group. Indeed, the experimental reaction kinetics were fully recapitulated by including the isomerization step in the RRKM/ME modelling.

The systems examined in this manuscript are direct models of free radical damaged peptides and fatty acids. Due to the prevalence of oxygen in the atmosphere and in the bio-molecular environment, it is conceivable that some of the mechanisms shown also occur in aqueous solution. Formation of carbonate radical anion is higher in energy than simple decomposition of the peroxyl adduct in aqueous solution to dioxygen and the fatty acid radical. Thus, the formation of carbonate radical anion is only expected to be favourable in the gas phase. In contrast, the novel decomposition pathway observed in the peptidic systems leading to loss of CO_2 and generation of $HO^{\bullet}$ is likely a competitive pathway in oxygenated aqueous solutions and is consistent with the products observed from gamma-irradiated peptides.

Acknowledgements

S.J.B., B.L.J.P., T.L., G.d.S and A.J.T acknowledge funding through the Australian Research Council (DP0986738, DP110103889 and DP1094135) and B.B.K. is supported by an Australian Postgraduate Award. S.J.B. and A.J.T. acknowledge the generous provision of computing resources from the NCI National Facility (Canberra) through the Merit Allocation Scheme and G.d.S. is thankful to the Victorian Partnership for Advanced Computing (VPAC) for providing computational resources. B.B.K. and S.J.B. thank Dr Shuji Kato (University of Colorado, Boulder) for helpful discussions and providing a SigmaPlot routine for calculation of collision rates.

References

1 P. D. Lightfoot, R. A. Cox, J. N. Crowley, M. Destriau, G. D. Hayman, M. E. Jenkin, G. K. Moortgat and F. Zabel, *Atmos. Environ.*, 1992, **26A**, 1805.
2 J. Zador, C. A. Taatjes and R. X. Fernandes, *Prog. Energy Combust. Sci.*, 2011, **37**, 371, DOI: 10.1016/j.pecs.2010.06.006.
3 B. Halliwell and J. M. C. Gutteridge, *Free radicals in biology and medicine*, OUP, Oxford, UK, 3rd edn, 1999.
4 B. J. Finlayson-Pitts and J. N. Pitts, *Science*, 1997, **276**, 1045.
5 B. F. Yates, W. J. Bouma and L. Radom, *Tetrahedron*, 1986, **42**, 6225.
6 H. Kenttämaa, *Ion-Molecule Reactions of Distonic Radical Cations*, in *Encyclopedia of Mass Spectrometry*, ed. N. M. M. Nibbering, Elsevier, Amsterdam, 2005, pp. 160–164.
7 B. B. Kirk, D. G. Harman and S. J. Blanksby, *J. Phys. Chem. A*, 2010, **114**, 1446–1456.
8 A. M. Knepp, G. Meloni, L. E. Jusinski, C. A. Taatjes, C. Cavallotti and S. J. Klippenstein, *Phys. Chem. Chem. Phys.*, 2007, **9**, 4315.
9 P. G. Wenthold and R. R. Squires, *J. Am. Chem. Soc.*, 1994, **116**, 11890–11897.
10 T. Ly and R. R. Julian, *J. Am. Chem. Soc.*, 2008, **130**, 351–358.
11 D. G. Harman and S. Blanksby, *Org. Biomol. Chem.*, 2007, **5**, 3495.
12 C. A. Horiuchi and J. Y. Satoh, *Chem. Lett.*, 1984, 1509–1510.
13 J. L. Belletire and D. F. Fry, *J. Org. Chem.*, 1987, **52**, 2549–2555.
14 T. Y. Kim, M. S. Thompson and J. P. Reilly, *Rapid Commun. Mass Spectrom.*, 2005, **19**, 1657–1665.
15 Q. Sun, H. Nelson, T. Ly, B. M. Stoltz and R. R. Julian, *J. Proteome Res.*, 2009, **8**, 958–966.
16 S. Gronert, *J. Am. Soc. Mass Spectrom.*, 1998, **9**, 845.
17 T. Su and W. J. Chesnavich, *J. Chem. Phys.*, 1982, **76**, 5183.
18 J. J. Grabowski and L. J. Zhang, *J. Am. Chem. Soc.*, 1989, **111**, 1193.

19 M. J. Frisch, G. W. Trucks, H. B. Schlegel, G. E. Scuseria, M. A. Robb, J. R. Cheeseman, G. Scalmani, V. Barone, B. Mennucci, G. A. Petersson, H. Nakatsuji, M. Caricato, X. Li, H. P. Hratchian, A. F. Izmaylov, J. Bloino, G. Zheng, J. L. Sonnenberg, M. Hada, M. Ehara, K. Toyota, R. Fukuda, J. Hasegawa, M. Ishida, T. Nakajima, Y. Honda, O. Kitao, H. Nakai, T. Vreven, J. A. Montgomery, Jr., J. E. Peralta, F. Ogliaro, M. Bearpark, J. J. Heyd, E. Brothers, K. N. Kudin, V. N. Staroverov, R. Kobayashi, J. Normand, K. Raghavachari, A. Rendell, J. C. Burant, S. S. Iyengar, J. Tomasi, M. Cossi, N. Rega, N. J. Millam, M. Klene, J. E. Knox, J. B. Cross, V. Bakken, C. Adamo, J. Jaramillo, R. Gomperts, R. E. Stratmann, O. Yazyev, A. J. Austin, R. Cammi, C. Pomelli, J. W. Ochterski, R. L. Martin, K. Morokuma, V. G. Zakrzewski, G. A. Voth, P. Salvador, J. J. Dannenberg, S. Dapprich, A. D. Daniels, Ö. Farkas, J. B. Foresman, J. V. Ortiz, J. Cioslowski and D. J. Fox, *GAUSSIAN 09 (Revision A.02)*, Gaussian, Inc., Wallingford CT, 2009.
20 L. A. Curtiss, P. C. Redfern, K. Raghavachari and J. A. Pople, *J. Chem. Phys*., 2001, **114**, 108.
21 J. Zheng, Y. Zhao and D. G. Truhlar, *J. Chem. Theory Comput*., 2009, **5**, 808.
22 (*a*) MultiWell-2010.1 Software, 2010, designed and maintained by John R. Barker with contributors Nicholas F. Ortiz, Jack M. Preses, Lawrence L. Lohr, Andrea Maranzana, Philip J. Stimac, T. Lam Nguyen, and T. J. Dhilip Kumar, University of Michigan, Ann Arbor, MI; http://aoss.engin.umich.edu/multiwell/; (*b*) J. R. Barker, *Int. J. Chem. Kinet*., 2001, **33**, 232; (*c*) J. R. Barker, *Int. J. Chem. Kinet*., 2009, **41**, 748; (*d*) T. L. Nguyen and J. R. Barker, *J. Phys. Chem. A*, 2010, **114**, 3718.
23 G. P. Smith and D. M. Golden, *Int. J. Chem. Kinet*., 1978, **10**, 489–501.
24 T. Tabarin, R. Antoine, M. Broyer and P. Dugourd, *Rapid Commun. Mass Spectrom*., 2005, **19**, 2883–2892.
25 W. M. Garrison, *Chem. Rev*., 1987, **87**, 381–398.
26 A. J. Chalk and L. Radom, *J. Am. Chem. Soc*., 1997, **119**, 7573–7578.
27 D. K. Bohme, *Int. J. Mass Spectrom. Ion Processes*, 1992, **115**, 95–110.
28 Interestingly this barrier is comparable to that calculated for the analogous proton transfer in the even-electron acetylglycinate anion itself (~8 kcal mol^{-1}, data not shown). This further supports the conclusion that in the oxygen-assisted pathway the radical does not play a direct role in the observed catalysis.
29 P. J. Barker, A. L. J. Beckwith and Y. Fung, *Tetrahedron Lett*., 1983, **24**, 97–100.
30 G. da Silva, J. W. Bozzelli, L. Liang and J. T. Farrell, *J. Phys. Chem. A*, 2009, **113**, 8923.
31 G. da Silva, *J. Phys. Chem. A*, 2011, **115**, 291.
32 G. da Silva, B. Z. Dlugogorski and E. M. Kennedy, *Int. J. Chem. Kinet*., 2007, **39**, 645.
33 $C_6(t) = \exp(-t/\tau_1)$; $C_7(t) = K_1 \exp(-t/\tau_1) + K_2 \exp(-t/\tau_2)$; $K_1 = \tau_2/(\tau_1 - \tau_2)$; $K_2 = \tau_2/(\tau_2 - \tau_1)$; $\tau_1 = 1/(k_3[O_2])$; $\tau_2 = 1/(k_5[O_2])$.
34 T. Ly and R. R. Julian, *Angew. Chem., Int. Ed*., 2009, **48**, 7130–7137.
35 H. G. Viehe, Z. Janousek, R. Merenyi and L. Stella, *Acc. Chem. Res*., 1985, **18**, 148–154.
36 G. P. F. Wood, D. Moran, R. Jacob and L. Radom, *J. Phys. Chem. A*, 2005, **109**, 6318–6325.
37 W. M. Garrison, M. Kland-English, H. A. Sokol and M. E. Jayko, *J. Phys. Chem*., 1970, **74**, 4506.
38 D. M. Tomazela, A. A. Sabino, R. Sparrapan, F. C. Gozzo and M. N. Eberlin, *J. Am. Soc. Mass Spectrom*., 2006, **17**, 1014–1022.